Received: 15 October 2020 | Revised: 17 February 2021 | Accepted: 7 March 2021

DOI: 10.1111/all.14851

Allergy EUROPEAN JOURNAL OF ALLERGY AND CLINICAL IMMUNOLOGY EAACI WILEY

ORIGINAL ARTICLE

Atopic Dermatitis, Urticaria and Skin Disease

Direct assessment of individual skin barrier components by electrical impedance spectroscopy

Roman Mannweiler[1] | Sophia Bergmann[2] | Sabine Vidal-y-Sy[2] | Johanna M. Brandner[2] | Dorothee Günzel[1]

[1]Institute of Clinical Physiology/Nutritional Medicine, Medical Department, Division of Gastroenterology, Infectiology, Rheumatology, Charité – Universitätsmedizin Berlin, Berlin, Germany

[2]Department of Dermatology and Venerology, University Hospital Hamburg-Eppendorf, Hamburg, Germany

Correspondence
Dorothee Günzel, Institute of Clinical Physiology/Nutritional Medicine, Medical Department, Division of Gastroenterology, Infectiology, Rheumatology, Charité – Universitätsmedizin Berlin, 12203 Berlin, Germany.
Email: dorothee.guenzel@charite.de

Funding information
This work was supported by the Deutsche Forschungsgemeinschaft [DFG GRK 2318, Project A1 (DG) and BR 1982-4/1 (JMB)].

Abstract

Background: Expression of the tight junction proteins Cldn1 and 4 is altered in skin diseases such as atopic dermatitis, and Cldn1 deficiency affects skin barrier formation. Impedance spectroscopy (IS) has been proven to allow detection of alterations in the skin barrier but is currently unable to separate effects on viable epidermis (VE) and stratum corneum (SC).

Methods: Effects of siRNA-mediated Cldn1 and 4 knockdown in reconstructed human epidermis (RHE) on VE and SC barrier function were investigated with Ussing chamber-based IS. Barrier components were sequentially altered, employing iron oxide nanoparticles and EGTA, to identify their contribution to the impedance spectrum. Resistance changes due to apically applied hyperosmolar electrolyte were used to identify barrier defects non-invasively.

Results: IS of RHE yielded two relaxation frequencies, representing the barrier properties of the SC (~1000 Hz) and VE (~100 Hz). As proof of concept, it was shown that the Cldn1 knockdown-induced resistance drop arises from the impairment of both SC and VE, indicated by a shift of both relaxation frequencies. Hyperosmolar electrolyte penetration allowed non-invasive detection of Cldn1 knockdown via time-dependent frequency shifts. The absence of Cldn4 knockdown-induced changes revealed the weaknesses of transepithelial electrical resistance analysis.

Conclusion: In conclusion, the present technique allows to separately measure the barrier properties of SC and VE and further evaluate the Cldn1 and 4 knockdown impact on the skin barrier. As the measurement with agarose-embedded electrolyte allowed non-invasive identification of the Cldn1 knockdown, this opens the way to detailed in vivo skin barrier assessment.

KEYWORDS
impedance spectroscopy, reconstructed human epidermis, skin barrier, tight junctions, transepithelial electrical resistance

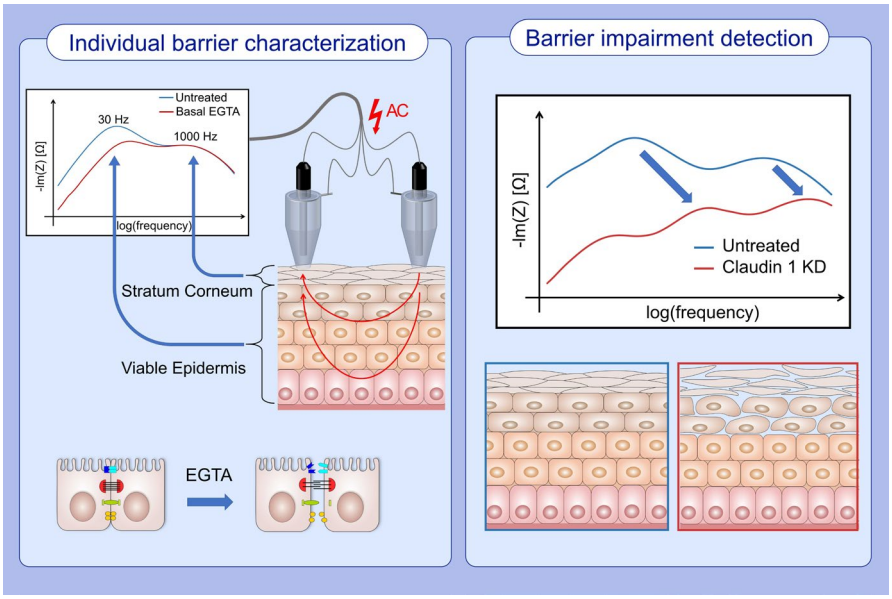

GRAPHICAL ABSTRACT

Impedance spectroscopy reveals optimum frequency ranges to measure the Stratum Corneum and Viable Epidermis barrier properties separately and non-invasively. EGTA induces resistance drop proofs that the viable epidermis contributes significantly to the overall epidermal barrier. The presented methods can detect barrier defects non-invasively ex vivo.

Abbreviations: AC, alternating current; EGTA, ethyleneglycol-bis(β-aminoethyl)-N,N,N′,N′-tetraacetic acid; Hz, hertz; KD, knock-down

1 | INTRODUCTION

The healthy epidermis provides a tight barrier against the intrusion of pathogens, toxins and allergens, but also against the unregulated loss of water. Whereas the stratum corneum (SC) has long been identified as an important component of the skin barrier,[1–4] it became clear during the past two decades that the tight junction also plays a role in skin barrier formation.[5,6] Several skin diseases, such as atopic dermatitis, contact dermatitis, psoriasis, various forms of inflammation and different types of skin cancer, are associated with impaired skin barrier function.[7–9] Especially in allergy-associated diseases, this facilitates the uptake of allergens and perpetuates a vicious circle. Disease-related alterations of SC components (eg of Filaggrin or ceramides) are well established.[7,10,11] However, many of these conditions are also accompanied by alterations in the expression of tight junction proteins in the viable epidermis (VE), especially the *stratum granulosum*. Particularly, a down-regulation of claudin-1 and -4 (Cldn1; Cldn4[6,12,13]; for review see[14,15]) was described. In vitro, mouse model and human skin studies demonstrated a correlation between the degree of Cldn1 down-regulation and the penetration of macromolecules of different sizes.[13,16] On the other hand, temporal, controlled opening of skin barrier may be desirable for dermal drug delivery.[17]

The development of efficient treatments for barrier-linked skin diseases and drug delivery optimization requires full understanding of the contribution of each component towards skin barrier function. The overall skin barrier function is often characterized via trans-epidermal water loss,[18] transepithelial electrical resistance,[19] skin permeation of locally applied drugs[20,21] and also impedance spectroscopy.[22,23] However, these techniques lack the ability of differentiating between barrier properties of the SC and viable epidermis (VE) including tight junctions. Removing the SC by tape stripping[24] or affecting it via electroporation[25] can evaluate its contribution to the barrier but may also damage the VE.

Impedance spectroscopy is a common method for characterizing the barrier function of monolayered epithelia.[26] Measuring transepithelial impedance over a range of frequencies gives rise to a curve which contains relaxation frequency peaks. The peak position and height are determined by distinct resistance and capacitance values of the specific cell type. Impedance spectra can be interpreted by analysing an equivalent circuit model, containing electrical components that represent the sample's response to the applied alternating current. Six basic components can approximate a monolayered epithelium: resistance and capacitance of apical and basal side, respectively, resistance of the tight junction and subepithelial resistance (Figure 1A).[27]

The present study aims to adapt the equivalent circuit model for use in stratified epithelia and thus allow to distinguish between SC and VE barrier components. As a proof of principle, the technique is used to distinguish between the effects of Cldn1 and 4 knockdown. We used reconstructed human epidermis (RHE), to have an easily adjustable model of the skin, that allows to univocally identify the skin barrier components. Our results promise the prospect of future adaptation of the technology for in vivo applications.

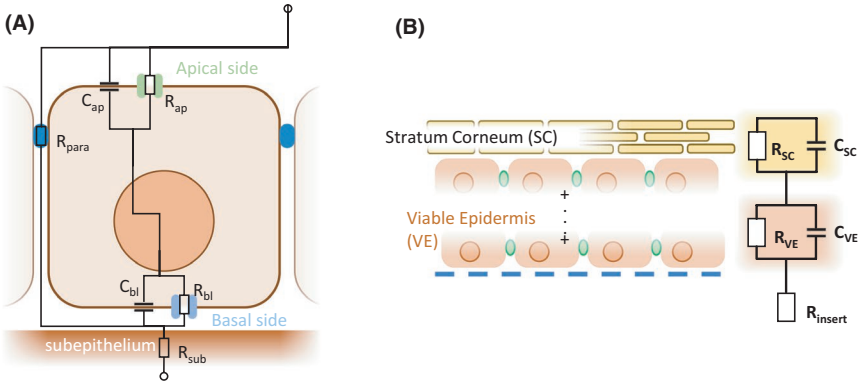

FIGURE 1 Equivalent circuit model of a cell monolayer. (A) Schematic illustration of a monolayered epithelium with its electric components. Ion passages are represented by resistors while lipid membranes act as capacitors. The tight junction is denoted as R_{para}, that is as the main resistor within the paracellular pathway. R_{ap}, C_{ap}, R_{bl} and C_{bl} are the resistances and capacitances of the apical and basolateral plasma membranes, respectively, R_{sub} is the resistance of the subepithelial tissues or filter supports. (B) Schematic illustration of reconstructed human epidermis, with a conceivable model of its electric components

2 | MATERIALS AND METHODS

2.1 | Materials

Standard bath solution contained (113.6 mM NaCl, 21 mM $NaHCO_3$, 2.4 mM Na_2HPO_4, 0.6 mM NaH_2PO_4, 5.4 mM KCl, 1.2 mM $CaCl_2$, 1.2 mM $MgCl_2$, 10 mM Glucose, equilibrated with 5% CO_2/ 95% O_2 to obtain a pH value of 7.4).

Mouse ear control treatment was performed with phosphate-buffered solution (PBS (+/+)) with calcium and magnesium (DPBS, GibcoTM—Thermo Fisher Scientific). Acetone (JT Baker—Fisher Scientific GmbH) was used to disrupt the skin barrier of mouse ears.

To disrupt the tight junction strands, a 0.1 M EGTA stock solution was prepared (EGTA (Merck) in ddH_2O titrated with 5 M NaOH to pH 7.0). To modulate SC capacitance, iron oxide nanoparticles (5 nm diameter, oleic acid functionalization, suspended in 10 ml toluene, Cytodiagnostics), Decamethylcyclopentasiloxane (TCI Chemicals, organic solvent commonly used in make-up removers) and a Neodymium magnet (10 mm diameter, 3 mm thickness, Webcraft GmbH) were used to coat the SC with the nanoparticles.

For cultivation of primary keratinocytes, human tissue was gained during surgical removal of foreskin anonymously from male donors (younger than 5 years; approved by the ethics committee of the Aerztekammer Hamburg, WF-61/12) gained during surgical removal of foreskin. All investigations were conducted according to the principles expressed in the Declaration of Helsinki.

siRNAs for human Cldn1 Hs_CLDN1_8: SI04279114, Cldn4 Hs CLDN4_7 (SI03064418) and AllStars negative control (siRNA ctrl; SI03650318) were purchased from QIAGEN (Hilden). Their effectiveness has been previously established.[13,28]

2.2 | Reconstructed human epidermis

Reconstructed human epidermis (RHE) was built essentially as described before.[14] 2 × 10^5 keratinocytes were seeded onto cell culture inserts (12 mm diameter, area 0.6 cm^2, 400 nm pore size, Merck Millipore) in 500 µl EpiLife Medium (Life Technologies) including 1.5 mM $CaCl_2$. The basal compartment was filled with 2.5 ml EpiLife medium. Cells were lifted to the air-liquid interface after 30 h and medium in the basal part of the well was exchanged with 1.5 ml of EpiLife medium containing 1.5 mM $CaCl_2$, 92 µg/ml ascorbic acid (Merck) and 10 ng/ml recombinant human keratinocyte growth factor (R&D Systems). Medium was changed every second day. Experiments were performed at day 4 and day 8 after air-liquid interface (see also[13,14]). For characterization of the RHE-system concerning morphology, proliferation, differentiation and barrier function, see REF.[13] According to those findings, model batches were only used for evaluation if the SC surface was dry and TER of the siRNA untreated models was >600 Ohm·cm^2.

2.3 | siRNA experiments

Confluent cells in passage 3 were trypsinized, resuspended in EpiLife medium with 1.5 mM $CaCl_2$ and subsequently transfected by using HiPerFect Transfection reagent (Qiagen, Hilden) at a cell density of 4 × 10^5/ml with a final siRNA concentration of 80 nM. Transfected cells were directly used to build RHEs. For evaluation of knockdown efficiency, see supporting information chapter 7.

2.4 | Mice

All experiments were performed in accordance with the German law on animal protection and approved by the Landesamt für Gesundheit und Soziales (LAGeSo), Berlin (T0256/16 and TCH 0012/20). Adult male and female mice (22–34 weeks old, C57Bl/6NCrl background, see supporting information chapter 6) were sacrificed, and organs were harvested for use in an unrelated experiment. The carcasses were then immediately used for application of impedance spectroscopy on ear skin as described below.

2.5 | Manipulation of electrical parameters

To identify the VE barrier component of the RHEs, 300 µl of the 0.1 M EGTA stock solution was applied to the basal (or apical) side of the Ussing chamber (final concentration 3 mM) to disassemble TJ strands and thus reduce the VE resistance.[29]

To coat the SC with iron oxide nanoparticles, the cell culture insert was removed from the Ussing chamber and placed in a cell culture incubator (37°C, 5% CO_2, 85% humidity). Nanoparticles resuspended in Decamethylcyclopentasiloxane were added to the apical side (Figure S1), and a magnet was placed under the insert for 10 min to enrich the iron oxide nanoparticles at the SC. Subsequently, the inserts were submerged in standard bath solution, causing the iron oxide nanoparticles solution to rise, as the Decamethylcyclopentasiloxane density is lower than that of water. Thus, only nanoparticles that attached to the SC remained.

Mouse ear skin was manipulated by wiping both sides of the ear pinnae 10 times with a cotton swab, soaked with the treatment solution. As a control PBS(+/+) was used while acetone and hyperosmolar 0.5 M KCl solution were supposed to cause changes in the barrier properties. Acetone as an amphiphilic compound was expected to destabilize the structures in the VE if capable of penetrating through the SC.

2.6 | Ussing chamber-based impedance spectroscopy

A standard Ussing chamber-based setup was used as described in Figure 2A.[26] The electric setup consists of two current electrodes (Working Electrode, Counter Electrode) and two reference electrodes (RE1, RE2).

For the alternating current (AC) impedance measurement, a 25 µA sinusoidal current was applied through the current electrodes while the reference electrodes recorded the resulting transepithelial voltage drop and phase angle using a Newtons 4th Ltd PSM1700 phase sensitive multimeter. Each spectrum consisted of 48 data points ranging from 1.3 Hz to 65 kHz. The calculated impedance values, Z, for individual frequency data points are complex numbers that can be either expressed as real (Re(Z)) and imaginary (Im(Z)) part or magnitude (|Z|) and phase shift (φ).

RHE models mounted in the Ussing chamber divided the chamber into a basal and an apical compartment. Both compartments were filled with 10 ml standard bath solution. Continuous perfusion was achieved via bubble lift. Once the RHE models had reached stable transepithelial resistance values, impedance spectra recordings were started.

2.7 | 'Static' Ussing chamber technique

The 'static' Ussing chamber aimed to transfer electric characteristics of a standard Ussing chamber to a solid electrode as is necessary for in vivo implementation. Therefore, standard bath solution was embedded in a 1% agarose gel in a 1.5 ml Eppendorf® tube. 'Static' in this context refers to the fact that there is no perfusion of the agarose-embedded electrolyte. Electrodes were attached as depicted in Figure 2B and C. The bottom of the Eppendorf tube was cut so that the exposed agar could be directly placed onto the air-exposed SC, while the basal side of the RHE was placed in bath solution. Thus, the RHE models could be measured under air-liquid interface conditions without being damaged or removed from their culture well (Figure 2B).

In addition to the steady-state measurements, time series of six impedance spectra (one spectrum/min) were recorded to investigate characteristic behaviour due to hydration of the SC.[30] To enhance the hydration-induced resistance drop, hyperosmolar 0.5 M KCl solution embedded in a 1% agarose gel was used for the apical side of the chamber.

One-sided 'static' Ussing chamber used the same principle as the 'static' measurement, but both sides of the chamber were attached to the SC (Figure 2D and E). This mimics the measurement under in vivo conditions where the basal side of the skin is not accessible. For a detailed description of the 'static' chambers, see Figure S2.

As a proof of principle for ex/in vivo application, mouse ear skin was measured with a special aligned setup based on the static Ussing chamber as shown in the supplement (Figure S7C and D). In the following, this setup is denoted as 'static mouse'. All impedance values were corrected by the measurement area of the corresponding chamber, which were 0.6 cm^2 for standard, 0.17 cm^2 for static and 0.07 cm^2 for one-sided static and static mouse Ussing chamber measurement. In the case of one-sided static RHE and static mouse skin measurements, the values were additionally corrected by a factor of 0.5 as the current passes the skin layers twice (Figure 2E).

2.8 | Impedance spectra evaluation

The general appearance and the interpretation principles of impedance spectra are explained in the supporting information chapter 1 (Figure S2). The spectra were fitted with appropriate equivalent circuit models (Figure 1B, supporting information chapter 1, Figure S2) using the EIS Analyzer software.[31]

To assess the effect of substances manipulating the electrical properties of the tissue, pairwise analysis was performed. The value $diff_R$ was calculated, describing the relative resistance change after treatment of the same sample:

$$\mathrm{diff}_R = \frac{R_0 - R_{\mathrm{treatment}}}{R_0}$$

Analogous calculations were carried out for capacitance changes. As the measured epithelia did not yield ideal capacitance behaviour, the extraction of the capacitance value was performed with the help of the so called constant phase element as described in the supporting formation chapter 1 (Figure S2).

FIGURE 2 Ussing chamber designs. (A) Standard Ussing chamber setup. 1: Acrylic glass Ussing chamber. 2: Cells on cell culture insert mounted vertically inside the chamber. 3: Bath solution inlet. 4: Bath solution outlet. 5: Heated water jacket as reservoir to keep the bath solution at 37°C. 6: Bath solution, mixing and rapid perfusion of the Ussing chamber is achieved by using a bubble lift. 7: Current injecting electrodes. 8: Reference voltage electrodes. 9: Differential amplifier calculating the potential difference. 10: Phase sensitive multimeter. Image (B) and scheme (C) of the 'static' Ussing chamber setup. Electrical current flow is narrowed down to the contact area at the SC. The second part of the chamber is placed in the bath solution. (D) One-sided 'static' setup and Scheme (E). Both parts of the chamber are attached to the SC

If equivalent circuit fitting was not sufficiently accurate, quantitative analysis of the spectra was performed by fitting the relaxation frequency peaks in the −Im(Z) versus $\log_{10}$(frequency) graph via Origin 2020 Peak Fitting tool (Figure S3). Here, only the position of the relaxation frequency f_i was taken into account for evaluation and not the peak amplitude, as the relaxation frequency is insensitive to changes in the electrode size and current pathway as long as the cells maintain their characteristics (supporting information chapter 1 and 4). The impact of 0.5 M KCl penetration on the spectrum was analysed by calculating the shift of the relaxation frequencies f_i before f_{i_0} and after $f_{i_{KCl}}$ KCl penetration:

$$\Delta f_i = \log_{10}(f_{i_{KCl}}) - \log_{10}(f_{i_0})$$

The transepithelial electrical resistance (TER) was evaluated by TER_{norm}, which is given by normalizing individual TER values by the maximum TER value of the RHE model batch.

2.9 | Statistical analysis

Statistical analysis was performed with GraphPad Prism 8.3.0 software. Data are expressed as a mean ± standard error of the mean (SEM). The sample size is annotated to each bar in the graphs. Unpaired student's *t* test was performed to compare values of different conditions. When multiple testing was performed, adjusted *p*-values were determined by Tukey's range test. The corresponding *p*-values are listed in the figure annotations.

3 | RESULTS

Many skin diseases comprise barrier defects. However, to which extent these defects concern the SC or the VE is often not clear. We used RHE as a model system for human skin which is easy to (genetically) manipulate and can also be prepared using cells from patients with skin diseases.[32] Currently, there is no convincing equivalent circuit model for skin that describes all barrier components and allows to choose the optimum frequency for measuring the desired barrier component. To draft such an equivalent circuit model (Figure 1B), potential barrier components were sequentially manipulated.

3.1 | Standard Ussing chamber technique

Impedance spectra of RHE measured in standard Ussing chambers yielded two predominant relaxation frequencies, in the range of 10 Hz to 100 Hz (f_{low}) and in the range of 500 Hz to 10,000 Hz (f_{high}) (Figure 3A). The absolute values of these frequencies remained unchanged over time (Figure 3B). Comparison of the fitting parameters resistance and capacitance over time (day 4 and day 8 after Ca^{2+} switch) showed an increase for the resistance value of f_{high} while its capacitance values dropped. There were no significant changes for f_{low} (Figure 3C and D).

Figure 3A also demonstrates that basally applied EGTA mainly affected f_{low} while f_{high} remained unchanged. Apically applied EGTA impacted f_{low} only slightly and f_{high} not at all (Figure 3A). Consistently, basal EGTA treatment caused the f_{low} resistance calculated by equivalent circuit fitting to drop significantly more than the f_{high} resistance, whereas there was no significant change for apical treatment (Figure 3E). For basal treatment no significant difference in capacitance change could be observed (Figure 3F). Furthermore, the relaxation frequency f_{low} was significantly higher after basal EGTA treatment.

Iron oxide nanoparticle deposition onto the SC affected predominantly f_{high} and in some cases f_{low} (Figure 4A), causing a significantly higher decrease of the capacitance value and increase of the resistance and relaxation frequency value for f_{high} compared with f_{low} (Figure 4B and C), leading to an overall increase of the frequency value for f_{high} (Figure 4D). Basal EGTA post-treatment only showed significant decrease of the relative resistance $diff_R$ (Figure 4E).

The absence of a significant increase of the f_{low} frequency value upon EGTA post-treatment and details on the effect of nanoparticle deposition are discussed in the supporting information.

In summary, EGTA acts on f_{low} when applied from basal side and predominantly affected its resistance and frequency value. The frequency shift of f_{low} is predominantly caused by the resistance drop. Iron oxide nanoparticle deposition on the SC (from apical side) mainly affected f_{high}, while f_{low} was also affected in some cases. Here, the frequency shift of f_{high} is dominated by the capacitance decrease. Throughout RHE cultivation, the capacitance dropped for f_{high} while its resistance increases. Together, this indicates that f_{low} represents the VE, f_{high} the SC.

3.2 | 'static' Ussing chamber technique

For a future in vivo implementation, the 'static' Ussing chamber technique was applied to RHE models and mouse ear pinnae.

The relaxation frequencies f_{low} and f_{high} were also detectable in static RHE, static one side RHE and static mouse skin (Figure 5A), with the latter yielding a lower relaxation frequency distance (exemplary spectra and fitting details see supporting information chapter 5). The

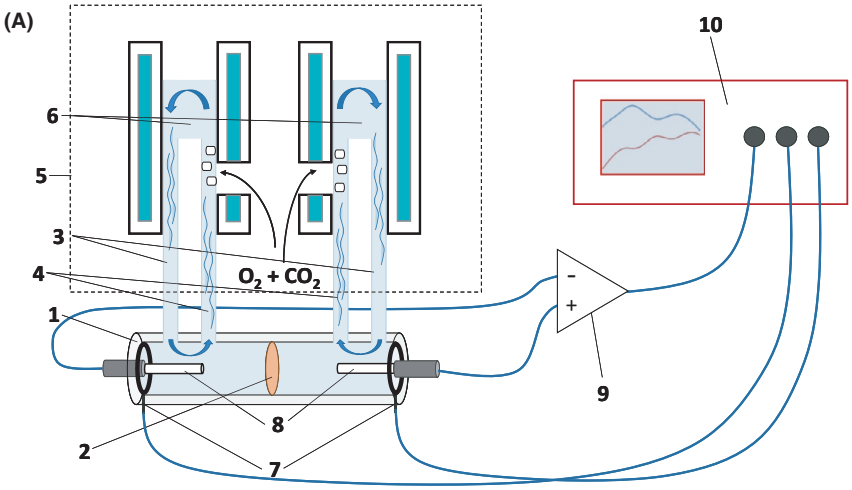

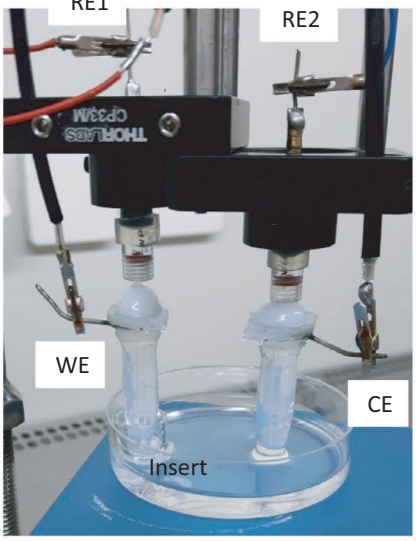

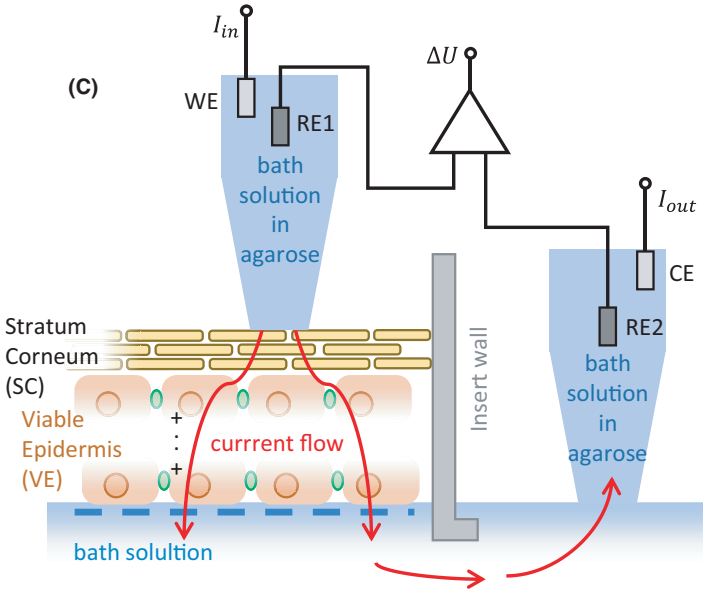

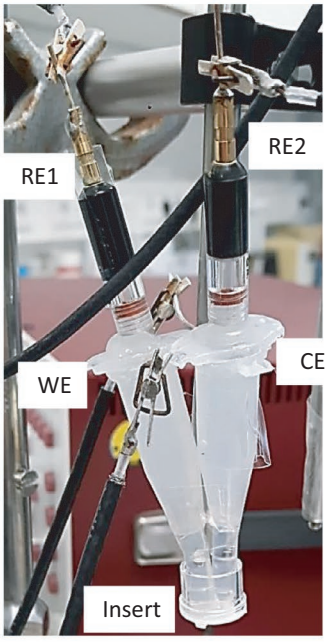

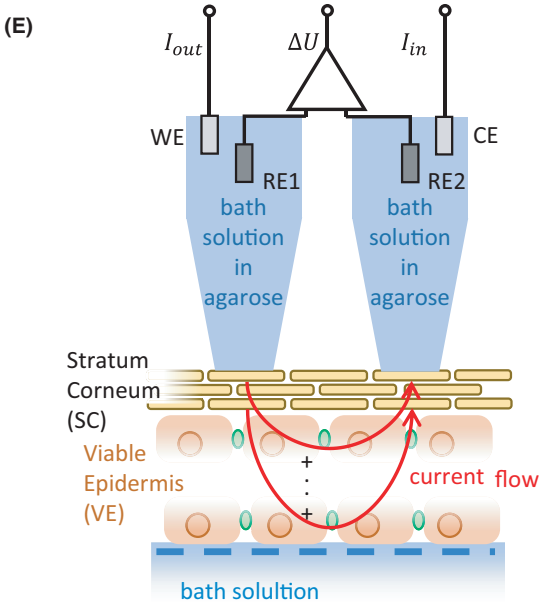

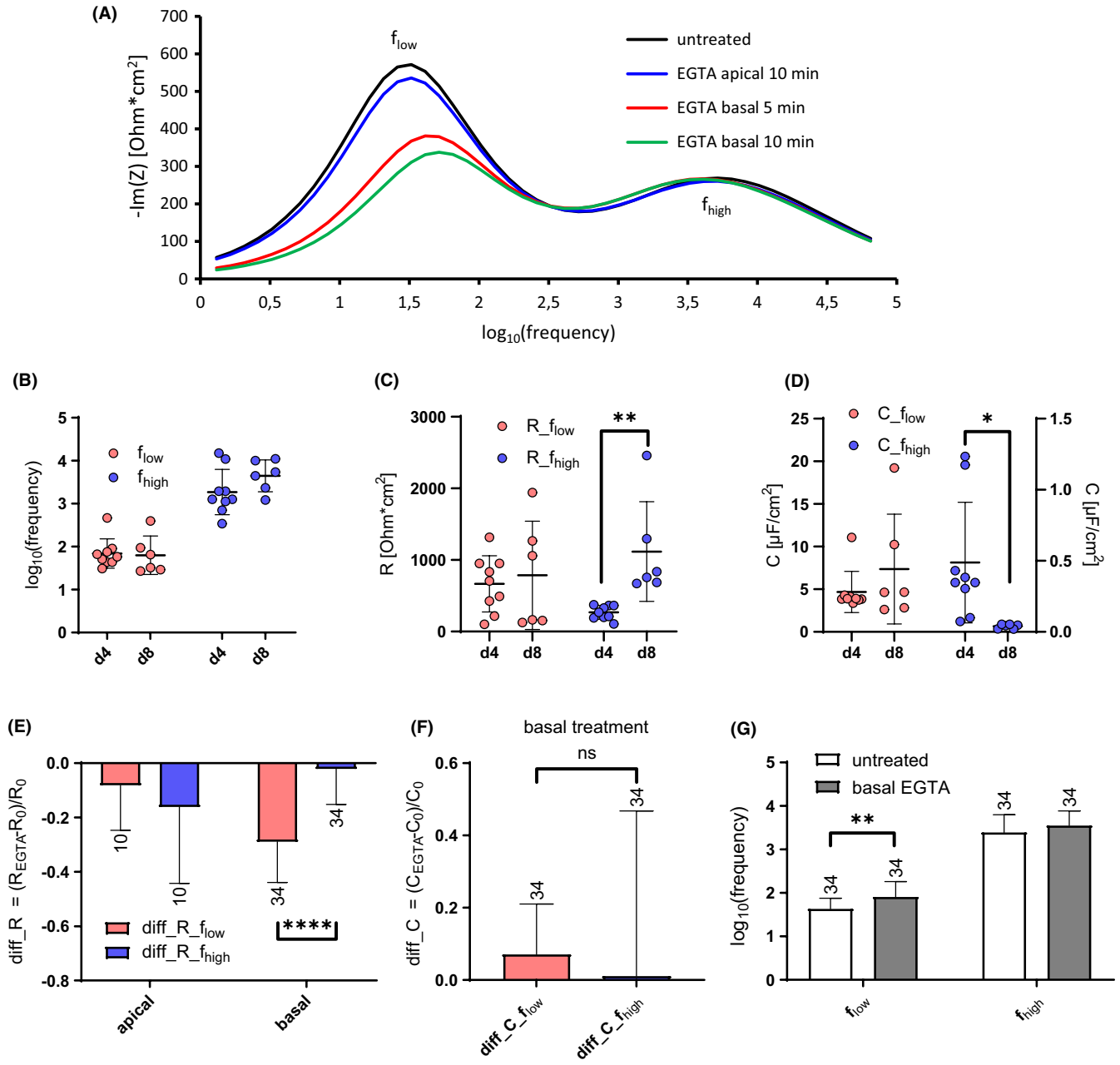

FIGURE 3 Effects of EGTA on RHE components. (A) Exemplary plot of negative imaginary part of the impedance −Im(Z) versus frequency showing the impact of EGTA application from apical and basal side on the impedance spectrum. Only the low relaxation frequency in the region of 10 Hz to 100 Hz appears to be affected by EGTA treatment. The effect can already be seen after 5 min of treatment. After 10 min, the additional impact on f_{low} is low with respect to the 5 min time point, thus indicating that the effect of EGTA is reaching an endpoint. (B) Frequency values for relaxation frequencies f_{low} and f_{high} remain unchanged over time (d4/8: day 4/8 after calcium switch). (C and D) Resistance and capacitance values for relaxation frequency f_{low} do not change over time. Resistance value for f_{high} increases significantly, while its capacitance value decreases. (D) Secondary axis shows values for f_{high}. (E) Impact of EGTA treatment from apical and basal side on resistance in RHE. Relative change of the resistance values before (R_0) and after 10 min (EGTA) treatment is shown. Only basal treatment showed significant difference in resistance change. (F) No significant capacitance (C) change before and after 10 min EGTA treatment could be observed. (G) The frequency value is significantly higher after basal EGTA treatment for relaxation frequency f_{low}. $^{*}p < 0.05$, $^{**}p < 0.01$, $^{****}p < 0.0001$; numbers at bars, n

peak heights −Im(Z) of f_{low} and f_{high} were significantly lower for the standard Ussing chamber measurement, whereas the −Im(Z(f_{high})) was much higher for the static mouse measurement (Figure 5B).

Time-resolved measurement of SC hydration, used as an alternative to the nanoparticle-based SC assignment in static RHE, showed a change in f_{high}, while f_{low} remained unchanged (Figure 5C). Alterations were mainly due to a decrease in R_{SC} (Figure 5D), with no change in the frequency. Subsequent basal application of EGTA was used to assure correct assignment of the relaxation frequencies for the static Ussing chamber setup (Figure 5C). Only f_{low} was affected

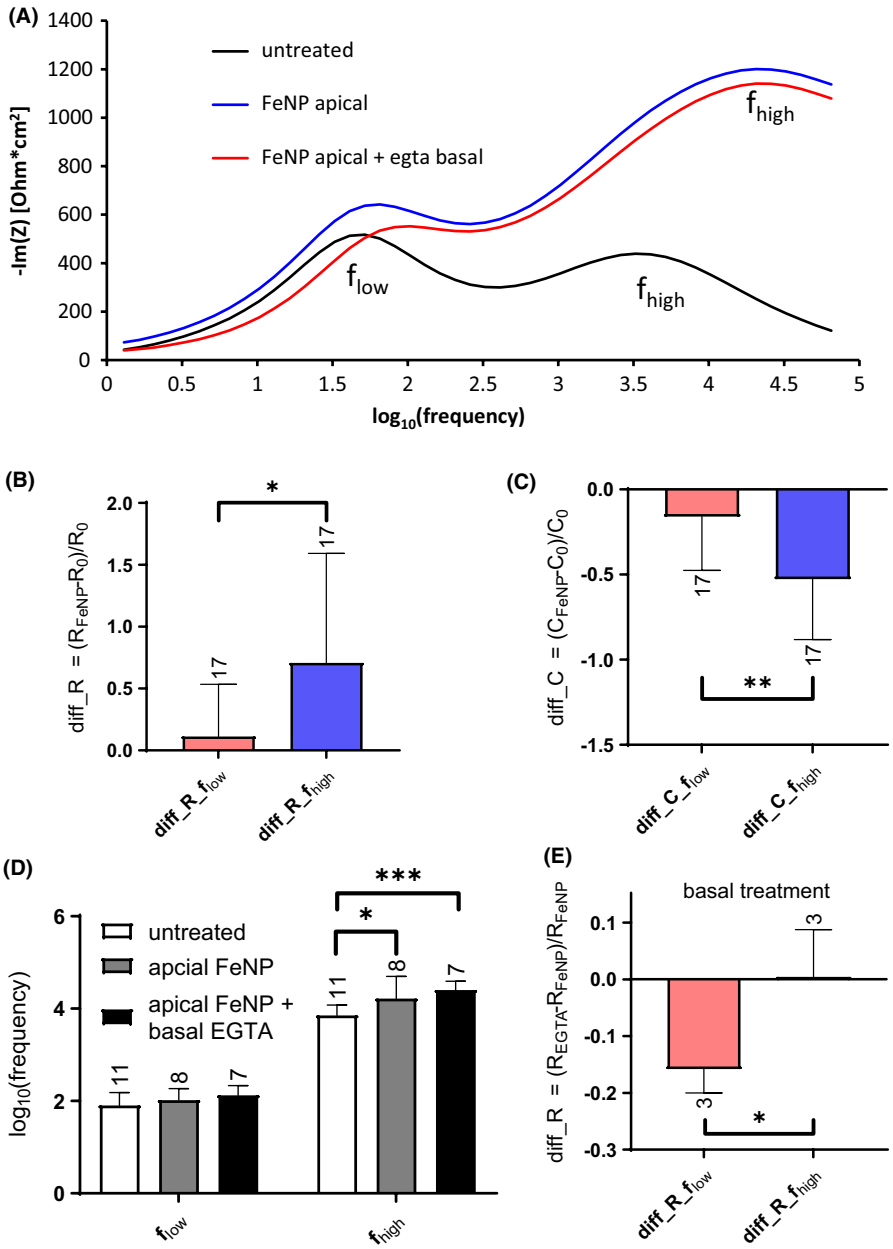

FIGURE 4 Effects of iron oxide nanoparticles on RHE components. Iron oxide nanoparticles (FeNP) were applied apically for 10 min (supporting information chapter 2) on RHE models followed by basal EGTA treatment for 10 min. (A) Exemplary graph showing the impact on the relaxation frequencies. FeNP causes major changes to f_{high} and minor to f_{low}, whereas EGTA acts only on f_{low}. (B and C) Impact of FeNP treatment on resistance (R) and capacitance (C) values. Graphs show the relative change of the resistance and capacitance values before (0) and after (FeNP) nanoparticle treatment. Resistance (B) increase and capacitance (C) decrease are significantly higher for f_{high}. (D) $\log_{10}$ of the frequency value shows no significant difference for f_{low} while for f_{high} it is significantly higher after apical nanoparticle (FeNP) treatment (E) Relative change of the resistance values of nanoparticle-treated RHE models (FeNP) after basal EGTA application. Resistance significantly drops for f_{low} after EGTA treatment. $^{*}p < 0.05$, $^{**}p < 0.01$, $^{***}p < 0.001$; numbers at bars, n

by basal EGTA treatment with the resistance decreased (Figure 5D) and frequency value increased (Figure 5E). Apical penetration of 0.5 M KCl, used to enhance the effect of SC hydration, resulted in a resistance change for both relaxation frequencies (Figure 5D) while a significant increase in the frequency value was only observed for f_{high} (Figure 5E).

When mouse ear skin was measured with the static Ussing chamber, f_{low} was only affected by acetone treatment, with its frequency value being significantly increased. For f_{high}, both acetone and 0.5 M KCl treatment increased the frequency value significantly, while PBS showed no effect (Figure 5F).

In summary, the frequencies found in the standard Ussing chamber could also be assigned with the static technique via SC hydration and basal EGTA treatment, that is f_{low} represents viable epidermis and f_{high} SC. Ex vivo testing with mouse ear skin showed that the relaxation frequencies found in RHE are also present in mouse ear skin and can be affected with acetone and 0.5 M KCl.

3.3 | Cldn knockdown evaluation

For standard Ussing chamber, spectra of RHE treated with different siRNAs and of untreated controls, normalized transepithelial resistance and relaxation frequency values were evaluated. Transepithelial resistance was significantly decreased for Cldn1 and Cldn4 knockdown compared to the control groups (Figure 6A). For Cldn1 knockdown, significant increase of the frequency values

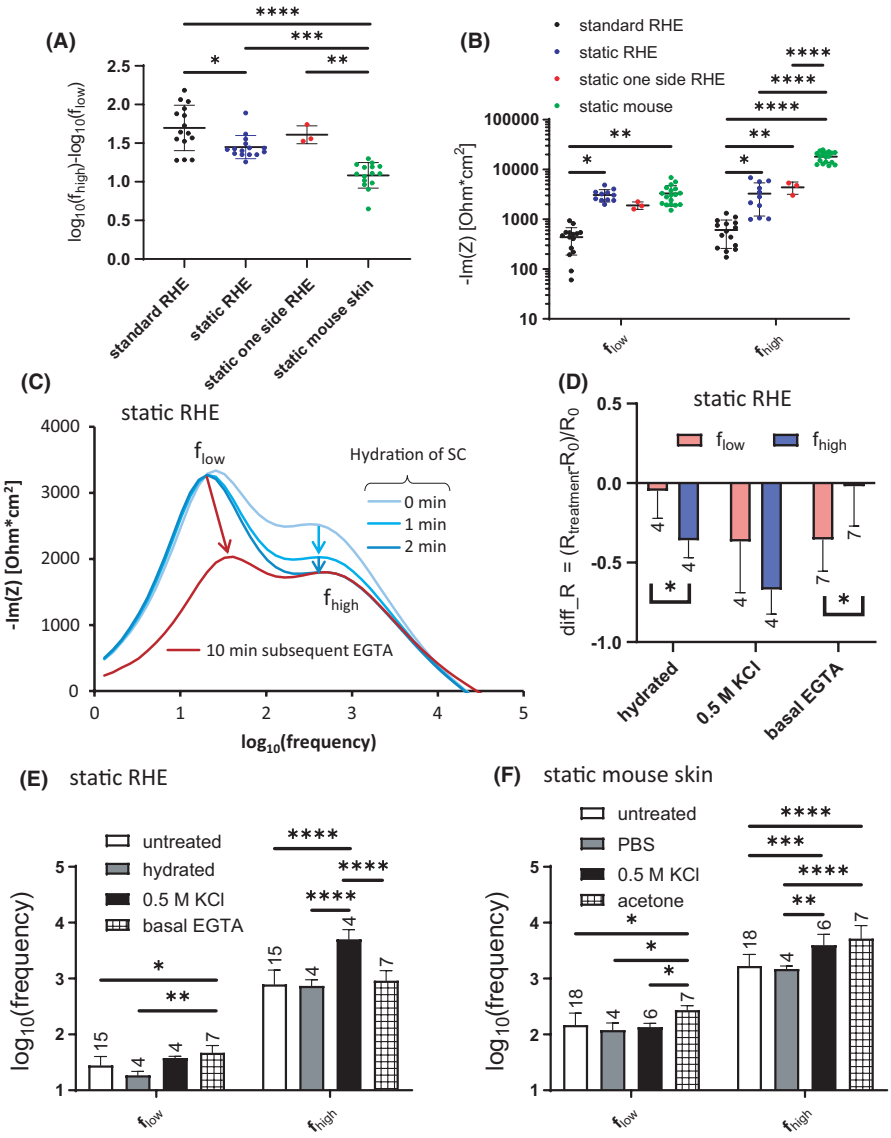

FIGURE 5 Comparison of standard and static Ussing chamber approaches. Different Ussing chamber setups (standard and static Ussing chamber) as well as different skin samples (RHE and mouse ear skin) were used. (A) Evaluation of the distance of the relaxation frequencies by subtracting the $\log_{10}$ (frequency) value of f_{low} from f_{high}. The distance is significantly lower for static mouse skin in comparison with the other measurements. (B) Evaluation of the peak height −Im(Z) for the corresponding relaxation frequencies. For f_{low}, only standard RHE yields significantly lower values. For f_{high}, standard RHE values are also significantly lower while static mouse yields much higher values. All values were corrected for the chamber measurement area. Static one-sided RHE and static mouse skin were additionally corrected by the factor 0.5, as the current passes two skin layers in these setups. (C) Exemplary spectra demonstrating the hydration of the SC upon static Ussing chamber attachment within 2 min. Only f_{high} appears to be affected by the hydration. 10 min of subsequent basal EGTA treatment only affected f_{low}. (D and E) Impact of Stratum Corneum (SC) hydration and basal EGTA treatment on RHE measured in static Ussing chamber. (D) Graphs show relative resistance change before (R_0) and after ($R_{treatment}$) the treatment. SC hydrated with bath solution causes significant resistance decrease for f_{high}. Hyperosmolar 0.5 M KCl penetration of SC affects both f_{low} and f_{high} with no significant difference between them. Basal EGTA significantly decreases the resistance for f_{low}. (E and F) Graphs show the $\log_{10}$ frequency value for the relaxation frequencies (RF) f_{low} and f_{high}. (E) For f_{low}, the RF value after basal EGTA treatment is significantly higher then untreated control and bath solution hydrated RHE. 0.5 M KCl treatment shows no significant differences to the other conditions. For f_{high}, the RF value is significantly higher after 0.5 M KCl treatment. (F) Impact of different apical treatments on mouse ear skin RF values measured with static Ussing chamber. For f_{low}, the RF value is significantly increased after acetone treatment. For f_{high}, both acetone and hyperosmolar 0.5 M KCl treatment increase the RF value significantly. PBS treatment shows no effect. $^*p < 0.05$, $^{**}p < 0.01$, $^{***}p < 0.001$, $^{****}p < 0.0001$; numbers at bars, *n*

was present for f_{low} (representing VE) and f_{high} (representing SC), whereas Cldn4 knockdown only shows slight changes in f_{low} (Figure 6B).

When using the static Ussing chamber technique, both the impact of hydration on the RHE model and the absolute values of the relaxation frequencies were evaluated (Figure 6A–D). In

these experiments, hyperosmolar 0.5 M KCl solution was used from apical side, to enhance the impact of hydration on the resistance. Comparing the first and last impedance spectra of the time series, the impact of KCl penetration differed between Cldn1 knockdown and untreated controls (Figure 6C and D). In untreated controls, only f_{high} was affected, whereas in Cldn1 knockdown f_{high} was only slightly affected and f_{low} highly. The ratio of the shift of f_{low} and f_{high} due to KCl penetration showed a significant difference for the Cldn1 knockdown (Figure 6E). Furthermore, there was a highly significant difference for the absolute values of the relaxation frequencies for Cldn1 knockdown in comparison to the other siRNA treatments (Figure 6F). This implicates that both barrier components have lower resistance and thus lower barrier integrity. In contrast to the transepithelial resistance evaluation in standard Ussing chamber, static Ussing chamber measurements showed no characteristic changes for the Cldn4 knockdown. This is further evaluated in supporting information chapter 4.

4 | DISCUSSION

The main goal of the present study was to draft an electrical model for the partial resistances of RHE and to evaluate the contribution of SC and VE to overall skin barrier function.

4.1 | Standard Ussing chamber

Standard Ussing chamber impedance spectra of stratified epithelia revealed two relaxation frequencies, f_{low} and f_{high}.

Basally applied EGTA allowed to assign f_{low} to the VE, as it only acts in viable tissue via tight junction strand disassembly[33] and ion channels activity (eg TRP channel).[34,35] The EGTA-induced frequency increase was attributed to a resistance drop in the VE and was used as a measure for barrier impairment.

Apical nanoparticle deposition not only added an additional layer on top of the SC but also altered its electric properties

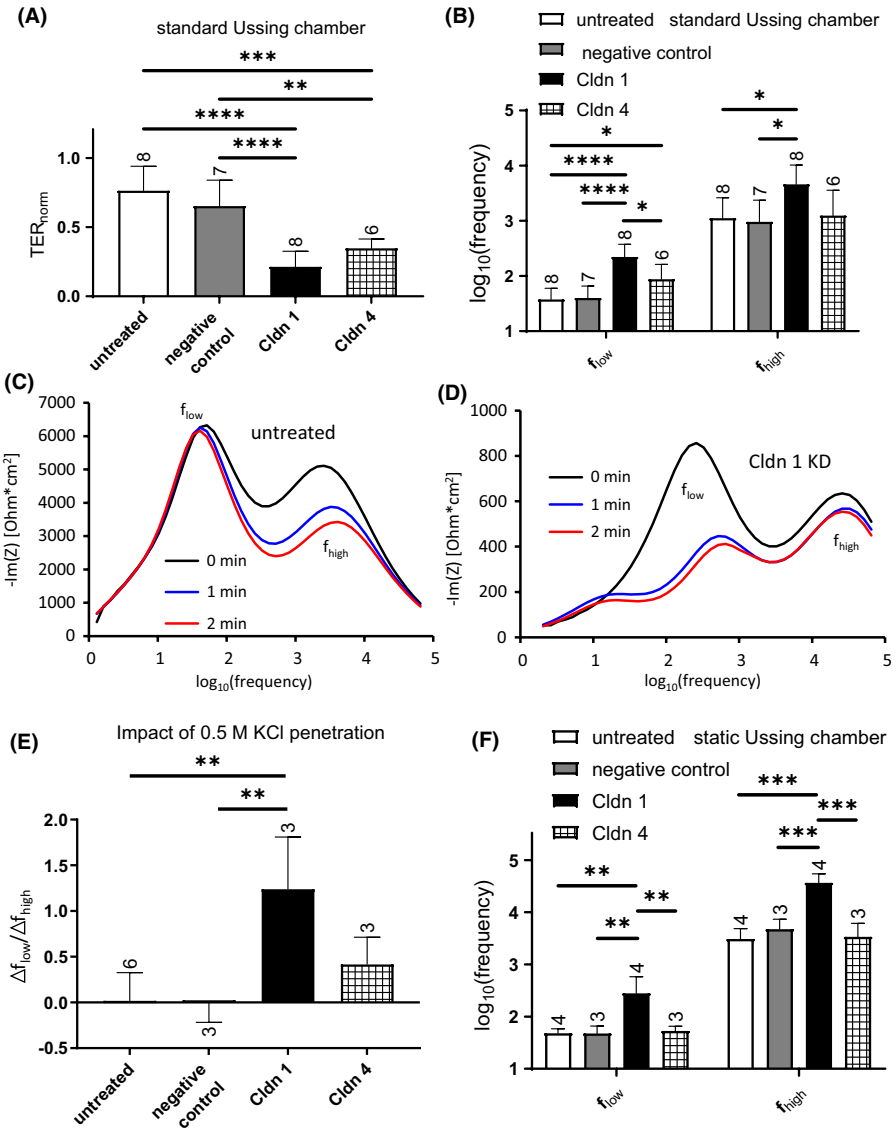

FIGURE 6 Effects of Cldn1 and Cldn4 knockdown. (A and B) Evaluation of RHE models measured with standard Ussing chamber. (A) Evaluation of impact of siRNA treatment on normalized transepithelial electrical resistance (TER_{norm}) shows significant differences for Cldn1 and Cldn4 compared to the control groups. 3 different batches of RHE models were measured on day 4 and day 8 after Ca^{2+} switch. (B) The same samples from (A) were evaluated for their relaxation frequencies. Significant increase was present for Cldn1 knockdown for both f_{low} and f_{high}, whereas Cldn4 knockdown caused significant increase in f_{low} only. (C–F) Evaluation of the siRNA treatment impact with static Ussing chamber techniques. One batch of RHE models at day 4 and 8 after Ca^{2+} switch was analysed. (C and D) Exemplary spectra over time during 0.5 M KCl penetration through the RHE model. (C) Only f_{high} is affected for the untreated control, while for Cldn1 knockdown (D) f_{low} is highly affected. (E) The ratio of the shifts Δf_{low} and Δf_{high} due to 0.5 M KCl penetration in RHE shows significant difference for Cldn1 knockdown. (F) Only Cldn1 knockdown relaxation frequencies significantly differ from the other treatments. $^{*}p < 0.05$, $^{**}p < 0.01$, $^{***}p < 0.001$, $^{****}p < 0.0001$

(supporting information chapter 2) thereby predominantly decreasing the capacitance, increasing the resistance and solely affecting the relaxation frequency value of f_{high}. Thus, f_{high} could be assigned to the SC.

Finally, the development of capacitance and resistance values over time supports the assignment of the relaxation frequencies. Decrease in the SC capacitance, increase in resistance and unchanged relaxation frequency $1/(R_{SC}{\cdot}C_{SC})$ over time were due to the increasing thickness of the SC.[13] Interestingly, no resistance increase or capacitance decrease could be observed for the VE over time. This is only possible if this relaxation frequency is predominantly represented by a barrier component with a fixed number of cells that do not change their properties over time and supports the finding that the main barrier forming tight junctions are found in a cell monolayer in the stratum granulosum.[3,4,36,37]

The absolute values of the relaxation frequencies for SC and VE did not change over time and thus are characteristic for the two barrier components identified here. The equivalent circuit analysis explained the origin of the frequency shift due to EGTA and nanoparticle application. For further analysis, the frequency shift could be used, as it is insensitive to changes in the electrode area.

4.2 | 'static' Ussing chamber

The standard Ussing chamber proved to be disadvantageous for applications on RHE (supporting information chapter 4, Figure S9). Yet, the assignment of the relaxation frequencies to the cellular barrier components VE and SC established with the standard Ussing chamber were validated for the static Ussing chamber via basal EGTA treatment and time-resolved hydration observation of the SC. EGTA decreased f_{low} resistance and frequency values while hydration solely affected the f_{high} resistance. Both components could also be identified in ex vivo mouse skin (Figure 5F, Figure S10E).

Using the static Ussing chamber technique in the one-sided configuration in RHE and for ex vivo mouse ear skin measurement maintained relaxation frequencies discovered with the standard Ussing chamber, thereby demonstrating the suitability for in/ex vivo applications. Higher impedance values for the SC of mouse ear skin are expected as in/ex vivo skin barrier is tighter than RHE barrier.[38] The differences in the frequency positions could be caused by an alternative current pathway such as sweat glands and hair follicles in the mouse ears acting as a shunt.

The ability to individually measure alterations in both SC and VE could be demonstrated under ex vivo conditions via acetone treatment which is a model for irritant dermatitis[39] and only SC via 0.5 M KCl treatment. The method thus allows to reassess previous in vivo approaches from the literature that were restricted to impedance measurements at 1 kHz.[23]

In summary, the 'static' technique has clear advantages over the commonly used techniques for transepithelial resistance measurement. Most importantly, the 'static' technique delivers separate information on the state of the VE and SC. The sample does not need to be submerged, so that the SC remains closer to its physiological state. The technique is independent of the insert used for RHE model cultivation as the area of current flow is limited by the electrode's geometry. When the electrolyte is prepared under sterile conditions, the technique can be used for sterile measurements.

4.3 | Cldn knockdown evaluation

Standard Ussing chamber measurements revealed significantly lower transepithelial resistance for Cldn1 and 4 knockdown, indicating a direct effect of these claudins on epidermal barrier function as has been shown previously in vivo and in vitro for Cldn1[3,13,16] and in 2D-cultures for Cldn4.[28,39] Furthermore, Cldn1 knockdown resulted in shifts of both relaxation frequencies, f_{low} (VE) and f_{high} (SC), to higher values while for Cldn4 knockdown only f_{low} (VE) is slightly altered.

The static Ussing chamber eliminated shunt contributions and verified characteristic frequency differences for the Cldn1 knockdown, but proved that Cldn4 knockdown did not result in any frequency changes (supporting information chapter 4 and Figure S11). Of note, no obvious skin barrier abnormalities were described in Cldn4 knockout mice.[40,41]

The shift of both relaxation frequencies to higher values and the lowered overall resistance indicates lower barrier integrity both in the SC and the VE caused by the absence of Cldn1, confirming previous studies on Cldn1-deficient mice.[12]

When considering implementing this technique for in vivo measurements, however, it will be problematic to rely on absolute resistance or relaxation frequency values, as these absolute values will vary for different individuals. This difficulty may be overcome by evaluating the time-dependent development of the spectra during penetration of hyperosmolar electrolytes. Under these conditions, we could identify Cldn1 knockdown-induced barrier defects in RHE by analysing the relaxation frequency shift without the need of a reference resistance or frequency value.

5 | CONCLUSION

The barrier properties of SC and VE of an epidermal stratified epithelium can be separately measured and individually characterized.

Cldn1-induced barrier defects can be identified by analysing the impact of hyperosmolar electrolyte penetration through the RHE model on the impedance spectrum over time. This demonstrates that tight junctions play an essential role in VE and thus in epidermal barrier function and opens up the possibility to exploit the present technique for a refinement of in vivo diagnostic tools for skin diseases with altered skin barrier such as allergic and irritant contact dermatitis.[15,42]

This may help to understand the contribution of barrier defects in SC and VE to different skin diseases and their endotypes in patients but also in various mouse models of skin diseases.[43,44]

ACKNOWLEDGEMENTS

We would like to thank Dr. Susanne M. Krug, Dr. Luca Meoli, and Germar Schüring for experimental support. Prof. Rolf Schuhmann's constructive and patient discussions are greatfully acknowledged.

CONFLICT OF INTEREST

Mr. Mannweiler has nothing to disclose. Dr. Bergmann has nothing to disclose. Ms. Vidal-y-Sy has nothing to disclose. Dr. Brandner reports grants from DFG (Deutsche Forschungsgemeinschaft) BR 1982-4/1, during the conduct of the study. Dr. Günzel reports grants from DFG (Deutsche Forschungsgemeinschaft) GRK 2318, during the conduct of the study.

AUTHOR CONTRIBUTIONS

Dorothee Günzel contributed to conceptualization, methodology, formal analysis, resources, writing—review and editing, supervision, project administration and funding acquisition. Johanna M. Brandner contributed to conceptualization, resources, writing—review and editing, supervision and funding acquisition. Roman Mannweiler contributed to methodology, validation, formal analysis, investigation, data curation, writing—original draft, writing—review and editing and visualization. Sabine Vidal-y-Sy contributed to resources, writing—review and editing. Sophia Bergmann contributed to resources, writing—review and editing.

ORCID

Roman Mannweiler https://orcid.org/0000-0001-5245-2007
Sophia Bergmann https://orcid.org/0000-0002-3743-5273
Dorothee Günzel https://orcid.org/0000-0002-7998-7164

REFERENCES

1. Proksch E, Brandner JM, Jensen J-M. The skin: an indispensable barrier. *Exp Dermatol*. 2008;17(12):1063-1072.
2. Lee AY. Molecular mechanism of epidermal barrier dysfunction as primary abnormalities. *Int J Mol Sci*. 2020;21(4):1194.
3. Furuse M, Hata M, Furuse K, et al. Claudin-based tight junctions are crucial for the mammalian epidermal barrier: a lesson from claudin-1-deficient mice. *J Cell Biol*. 2002;156(6):1099-1111.
4. Tunggal JA, Helfrich I, Schmitz A, et al. E-cadherin is essential for in vivo epidermal barrier function by regulating tight junctions. *EMBO J*. 2005;24(6):1146-1156.
5. Bäsler K, Bergmann S, Heisig M, Naegel A, Zorn-Kruppa M, Brandner JM. The role of tight junctions in skin barrier function and dermal absorption. *J Controlled Release*. 2016;242:105-118.
6. Yokouchi M, Kubo A. Maintenance of tight junction barrier integrity in cell turnover and skin diseases. *Exp Dermatol*. 2018;27(8):876-883.
7. Weidinger S, Novak N. Atopic dermatitis. *Lancet (London, England)*. 2016;387(10023):1109-1122.
8. Proksch E, Dähnhardt D, Dähnhardt-Pfeiffer S, Fölster-Holst R. Epidermal barrier disorders in dermatoses. *Hautarzt*. 2016;67(11):907-921.
9. Schmuth M, Blunder S, Dubrac S, Gruber R, Moosbrugger-Martinz V. Epidermal barrier in hereditary ichthyoses, atopic dermatitis, and psoriasis. *J Dtsch Dermatol Ges*. 2015;13(11):1119-1123.
10. Kezic S, Novak N, Jakasa I, et al. Skin barrier in atopic dermatitis. *Front Biosci*. 2014;19:542-556.
11. Koppes SA, Engebretsen KA, Agner T, et al. Current knowledge on biomarkers for contact sensitization and allergic contact dermatitis. *Contact Dermatitis*. 2017;77(1):1-16.
12. Sugawara T, Iwamoto N, Akashi M, et al. Tight junction dysfunction in the stratum granulosum leads to aberrant stratum corneum barrier function in claudin-1-deficient mice. *J Dermatol Sci*. 2013;70(1):12-18.
13. Bergmann S, von Buenau B, Vidal-y-Sy S, et al. Claudin-1 decrease impacts epidermal barrier function in atopic dermatitis lesions dose-dependently. *Sci Rep*. 2020;10(1):2024.
14. Basler K, Brandner JM. Tight junctions in skin inflammation. *Pflugers Arch*. 2017;469(1):3-14.
15. Brandner JM, Zorn-Kruppa M, Yoshida T, Moll I, Beck LA, De Benedetto A. Epidermal tight junctions in health and disease. *Tissue Barriers*. 2015;3(1–2):e974451.
16. Tokumasu R, Yamaga K, Yamazaki Y, et al. Dose-dependent role of claudin-1 in vivo in orchestrating features of atopic dermatitis. *Proc Natl Acad Sci*. 2016;113(28):E4061-E4068.
17. Benson HAE, Grice JE, Mohammed Y, Namjoshi S, Roberts MS. Topical and transdermal drug delivery: from simple potions to smart technologies. *Curr Drug Deliv*. 2019;16(5):444-460.
18. Alexander H, Brown S, Danby S, Flohr C. Research techniques made simple: transepidermal water loss measurement as a research tool. *J Invest Dermatol*. 2018;138(11):2295-2300.e2291.
19. Kiesewetter L, Littau L, Walles H, Boccaccini AR, Groeber-Becker F. Reepithelialization in focus: non-invasive monitoring of epidermal wound healing in vitro. *Biosens Bioelectron*. 2019;142:111555.
20. Pradal J, Vallet CM, Frappin G, Bariguian F, Lombardi MS. Importance of the formulation in the skin delivery of topical diclofenac: not all topical diclofenac formulations are the same. *J Pain Res*. 2019;12:1149-1154.
21. Shan J, Oshima T, Chen X, Fukui H, Watari J, Miwa H. Trypsin impaired epithelial barrier function and induced IL-8 secretion through basolateral PAR-2: a lesson from a stratified squamous epithelial model. *Am J Physiol*. 2012;303(10):G1105-G1112.
22. Ollmar S, Grant S. Nevisense: improving the accuracy of diagnosing melanoma. *Melanoma Manag*. 2016;3(2):93-96.
23. Rinaldi AO, Morita H, Wawrzyniak P, et al. Direct assessment of skin epithelial barrier by electrical impedance spectroscopy. *Allergy* 2019;74(10):1934-1944.
24. Bashir SJ, Chew A-L, Anigbogu A, Dreher F, Maibach HI. Physical and physiological effects of stratum corneum tape stripping. *Skin Res Technol*. 2001;7(1):40-48.
25. Lu F, Wang C, Zhao R, et al. Review of stratum corneum impedance measurement in non-invasive penetration application. *Biosensors*. 2018;8(2):31.
26. Gitter AH, Schulzke J-D, Sorgenfrei D, Fromm M. Ussing chamber for high-frequency transmural impedance analysis of epithelial tissues. *J Biochem Biophys Methods*. 1997;35(2):81-88.
27. Günzel D, Zakrzewski SS, Schmid T, et al. From TER to trans- and paracellular resistance: lessons from impedance spectroscopy. *Ann N Y Acad Sci*. 2012;1257(1):142-151.
28. Kirschner N, Rosenthal R, Furuse M, Moll I, Fromm M, Brandner JM. Contribution of tight junction proteins to ion, macromolecule, and water barrier in keratinocytes. *J Invest Dermatol*. 2013;133(5):1161-1169.
29. Tria S, Jimison LH, Hama A, Bongo M, Owens RM. Sensing of EGTA mediated barrier tissue disruption with an organic transistor. *Biosensors*. 2013;3(1):44-57.
30. Tagami H, Ohi M, Iwatsuki K, Kanamaru Y, Yamada M, Ichijo B. Evaluation of the skin surface hydration in vivo by electrical measurement. *J Invest Dermatol*. 1980;75(6):500-507.

31. Johnson P. Progress in chemometrics research, A. L. Pomerantsev (ed.), Nova Science, New York, 2005, ISBN 1-59454-257-0, vii +325, pp. *J Chemom*. 2005;19(4):266-267.
32. Niehues H, Bouwstra JA, El Ghalbzouri A, Brandner JM, Zeeuwen P, van den Bogaard EH. 3D skin models for 3R research: the potential of 3D reconstructed skin models to study skin barrier function. *Exp Dermatol*. 2018;27(5):501-511.
33. Rothen-Rutishauser B, Riesen FK, Braun A, Günthert M, Wunderli-Allenspach H. Dynamics of tight and adherens junctions under EGTA treatment. *J Membr Biol*. 2002;188(2):151-162.
34. Toth BI, Olah A, Szollosi AG, Biro T. TRP channels in the skin. *Br J Pharmacol*. 2014;171(10):2568-2581.
35. Bodding M, Wissenbach U, Flockerzi V. The recombinant human TRPV6 channel functions as Ca^{2+} sensor in human embryonic kidney and rat basophilic leukemia cells. *J Biol Chem*. 2002;277(39):36656-36664.
36. Kirschner N, Houdek P, Fromm M, Moll I, Brandner JM. Tight junctions form a barrier in human epidermis. *Eur J Cell Biol*. 2010;89(11):839-842.
37. Yoshida K, Yokouchi M, Nagao K, Ishii K, Amagai M, Kubo A. Functional tight junction barrier localizes in the second layer of the stratum granulosum of human epidermis. *J Dermatol Sci*. 2013;71(2):89-99.
38. Abd E, Yousef SA, Pastore MN, et al. Skin models for the testing of transdermal drugs. *Clin Pharmacol*. 2016;8:163-176.
39. Nakajima M, Nagase S, Iida M, et al. Claudin-1 binder enhances epidermal permeability in a human Keratinocyte model. *J Pharmacol Exp Ther*. 2015;354(3):440-447.
40. Kage H, Flodby P, Gao D, et al. Claudin 4 knockout mice: normal physiological phenotype with increased susceptibility to lung injury. *Am J Physiol Lung Cell Mol Physiol*. 2014;307(7):L524-L536.
41. Fujita H, Hamazaki Y, Noda Y, Oshima M, Minato N. Claudin-4 deficiency results in urothelial hyperplasia and lethal hydronephrosis. *PLoS One*. 2012;7(12):e52272.
42. Zhai H, Leow YH, Maibach HI. Human barrier recovery after acute acetone perturbation: an irritant dermatitis model. *Clin Exp Dermatol*. 1998;23(1):11-13.
43. Czarnowicki T, He H, Krueger JG, Guttman-Yassky E. Atopic dermatitis endotypes and implications for targeted therapeutics. *J Allergy Clin Immunol*. 2019;143(1):1-11.
44. Werfel T, Allam J-P, Biedermann T, et al. Cellular and molecular immunologic mechanisms in patients with atopic dermatitis. *J Allergy Clin Immunol*. 2016;138(2):336-349.

SUPPORTING INFORMATION

Additional supporting information may be found online in the Supporting Information section.

How to cite this article: Mannweiler R, Bergmann S, Vidal-y-Sy S, Brandner JM, Günzel D. Direct assessment of individual skin barrier components by electrical impedance spectroscopy. *Allergy*. 2021;76:3094–3106. https://doi.org/10.1111/all.14851